Dynamics analysis and experiment research of vibration response for dual-rotor system under rubbing fault

Nanfei Wang[1], Dongxiang Jiang[1]

[1] State Key Laboratory of Control and Simulation of Power System and Generation Equipment, Department of Thermal Engineering, Tsinghua University, Beijing 100084, China
wnf14@mails.tsinghua.edu.cn, jiangdx@tsinghua.edu.cn

Abstract

Rub-impact is one of the most common faults in aero-engine, which would cause excessive vibration and reduce the equipment performance, so it's important to investigate and recognize rubbing fault mechanism precisely in rotating machines. Also, as for aero-engine, dual-rotor system has been widely used to improve structure compact and efficiency. However, due to complex structure, it is of crucial importance to investigate the dual-rotor system of rubbing coupling faults mechanism for safe and steady running of aero-engine. In this paper, a new rotor-ball bearing coupling system with rub-impact fault is established for aero-engine. The nonlinear factors of ball bearing including the clearance of bearing and nonlinear Hertzian contact between balls and races are modelled. Moreover, the numerical integral method is utilized to obtain the vibration response under rub-impact condition. By means of the dual-rotor experiment rig, the rubbing experiments are conducted. The simulation results are found in highly consistent with the experimental results, which fully verified the effectiveness of the new rubbing model.

1 Introduction

In rotating machinery, in order to achieve the energy efficiency targets, it is common practice to reduce the clearance between the rotor and stator. However, the smaller the clearance of the rotating machinery is, the more the possibility of rub occurs. The rub-impact has long been identified as one of the most typical fault in the rotor system, which may cause catastrophic consequences and short service life [1].

Because of the complexity of the rubbing phenomenon, many scholars have paid more attention to the research of rub-impact phenomena. Muszynska [2] reviewed existing articles on the rubbing phenomenon and discussed the vibration response, such as impacting, friction, stiffness and coupling effects. Ahmad [3] illustrateed the influence of different system variables on the rotor dynamics, including stiffness, damping, acceleration of rotor, support structure asymmetry, thermal effects and disk flexibility etc. Choi [4] investigated the whirling motion of full annular rotor rub and explained the onset of the synchronous full angular rubbing fault. Beatty [5] proposed a widely accepted mathematical model for rub-impact forces and a detailed response format of diagnostic data in actual cases. Ma et al. [6] performed a theoretical analysis on the dynamic characteristics of a rotor-stator system under different rubbing forms. Zhang [7] analysed the dynamic characteristics of a micro-rotor system under rub-impact and presented the influences of model parameters, such as rotational speed, imbalance and damping. Taking into account the transient response of an supercritical high-speed rotor, Grapis et al. [8] discussed a number of rotor-stator collisions succeeded by full annular rub induced by a rapid increase of unbalance. Torkhani et al. [9] studied the partial rub of a rotor when rub-impact occurred between the rotor and the non-rotating obstacle under partial light, medium and severe rub conditions. Wang et al. [10, 11] analysed the dynamic characteristics of rotor system and the casing responses under rub-impact condition by using finite element method, envelop demodulation and empirical mode decomposition. Patel et al. [12] proposed a mathematic model composed of rotor and stator and investigated the nonlinear lateral-torsional vibration characteristics of a rotor under rub-impact with a viscoelastically suspended stator. For a turbo-generator model, Roques et al. [13] analysed the speed transients of rub-impact, which results from an accident blade-off imbalance. Yuan et al. [14] proposed a full-degree-of-freedom dynamic model for a Jeffcott rotor and analysed the effect of radial rub-impact on imbalance responses. Popprath and Ecker [15] investigated the intermittent contact of Jeffcott rotor system between the rotor and stator via nonlinear contact forces. Lu and Chu [16] investigated the dynamics characteristics, whirl and torsional vibrations of a vertical Jeffcott rotor under no rub, full annular rub and partial rub conditions.

Nowadays, in order to improve energy efficiency and higher thrust to weight ratio, dual-rotor systems are widely used in rotating machinery, such as aero-engine, gas turbine and nuclear reactors. In comparison with

single-rotor systems, not less than two excitation sources make dual-rotor systems exhibit complicated dynamic behaviour, especially for the system including nonlinear characteristics, for example rub-impact. In the aforementioned literature, the research emphasis is on the single-rotor system, which is obviously different from actual aero-engine. The major difference between dual-rotor system and single-rotor system is the involvement of inter-shaft bearing, which completes the coupling between outer rotor and inner rotor.

In the paper, a dual-rotor system capable of describing the mechanical vibration caused by rubbing fault is established, in which the compressor disk and turbine disk are considered in both inner rotor and outer rotor. Considering the soften characteristics of stator, the Lankarani-Nikravesh model is used to describe the impact force between the disk and fixed limiter. The numerical integral method is applied to obtain system's dynamic response, and the characteristics about the coupling faults are analysed by time-domain waveform and spectrum cascades. Finally, the experimental study is conducted on a dual-rotor test rig and the validity of the dual-rotor system dynamics model is verified by comparing with the experimental results.

2 Mathematical modelling of dual-rotor system

2.1 Rotor system model

The dual-rotor system with unbalance-rubbing coupling faults is presented in Figure 1, which consists of a low pressure rotor (rotor 1, node 1 to node 5) with a lower rotating speed, a high pressure rotor (rotor 2, node 6 to node 9) with a high rotating speed and a fixed limiter. There are four bearings included in the model, in which bearing 3 represents the inter-shaft bearing. The disks 1-4, located, respectively at node 2, node 4, node 7 and node 9, represent the concentrations of low-pressure compressor disk, low-pressure turbine disk, high-pressure turbine disk and high-pressure compressor disk. Rub-impact between the higher pressure rotor and the fixed limiter existed in the lateral direction of high-pressure turbine disk is shown to study the nonlinear dynamical response of the system. It is supposed that the lumped masses at every lumped mass point arem_i (i=1⋯9), the corresponding damping coefficients of which are c_i (i=1⋯9), respectively. k_i (i=1⋯7) are the stiffness coefficients of shaft segments, respectively. In order to investigate the dynamic characteristics of the dual-rotor model, the following assumptions are employed:

(a) Deformation of rotor and stator caused by rub-impact is considered infinitely small.
(b) The turbine disks and compressor disks of the dual-rotor system are rigid and represented by four lumped masses.
(c) To model contact friction forces, supposed that the rotor never sticks to the stator and always slips due to high rotating speed, and the effects of thermal and friction torque in rubbing are neglected.
(d) The material properties of rotors and stator are linear and elastic.
(e) Interaction of the fluid between the rotor and the stator is ignored.
(f) For the dual-rotor model established in the paper, the low-pressure and high-pressure shafts are not very long and slender, the effect of torsion is neglected.

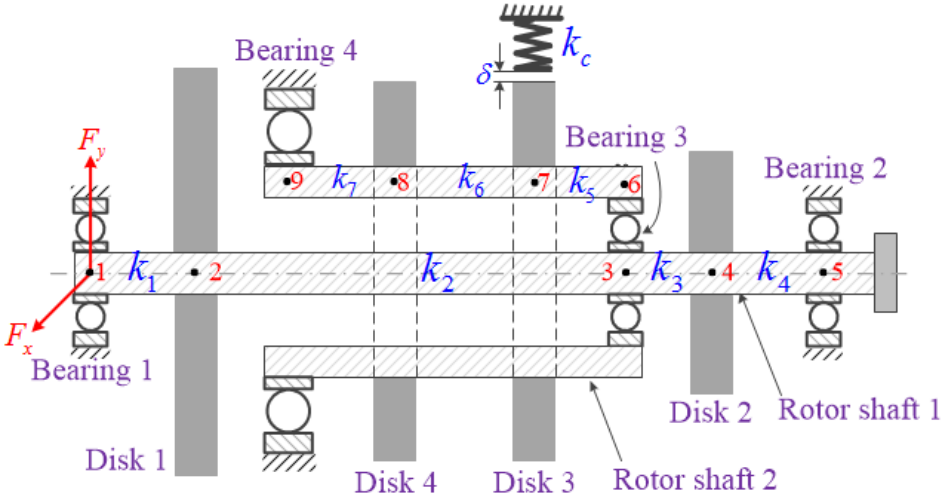

Figure 1 Mechanical model of the dual-rotor system

2.2 Fixed-point rubbing force model

Based on the assumptions, the stiffness of disk is greater than the rigidity of the stator. Therefore, it can be assumed that the deformation just occurs on the fixed limiter. In contrast with the complete rotation

period, the rub-impact time is so short that the impact between the rotor and limiter can be treated as a point-point contact. The master body is defined as the rotor and the slave one is the limiter. In the above assumptions, the rub-impact form is considered as local contact and the schematic diagram of rub-impact between the rotor and fixed limiter are presented in Figure 2, where $r = \sqrt[2]{x^2 + y^2}$ represents the radial displacement of the rotor relative to the limiter; F_N and F_τ denote the impact force and the tangential friction force under rub-impact condition, respectively; m denotes the mass of disk; K_r, c_r are the stiffness and damping ratio of rotor, respectively; k_c denotes the functional radial stiffness coefficient of fixed limiter; δ represents the clearance between the disk and fixed limiter; e is the mass eccentricity of the disk; (x, y) is defined the disk axis position, and $\varphi = arctan\,(y/x)$.

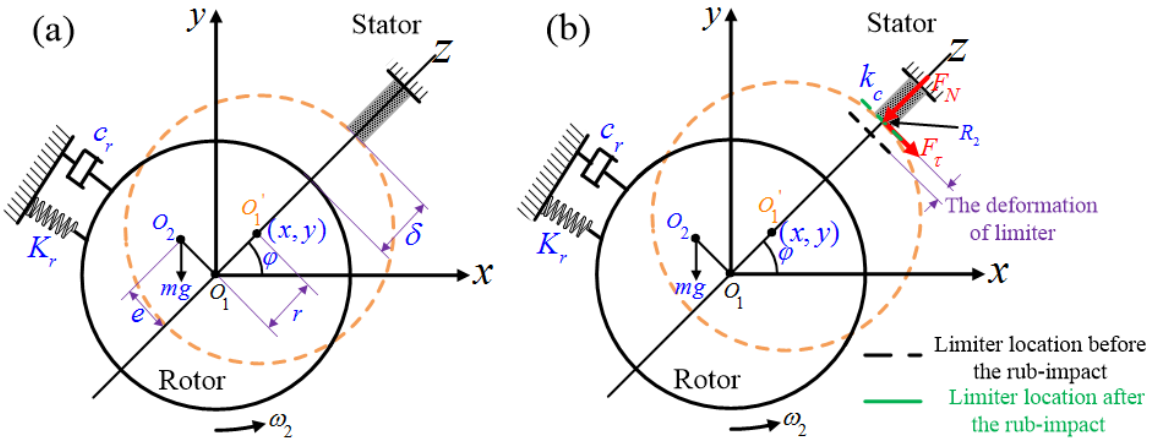

Figure 2 Schematic diagram of radical rub-impact between the rotor and stator

Considering the relatively soft material property of limiter, the Lankarani-Nikravesh model is utilized to describe the rub-impact force between the disk and limiter [26, 27]. The friction relationship under rubbing condition conforms to the Coulomb friction law, which is still one of the most widely used models to describe the friction phenomenon. Let f represents the friction factor, and the normal and tangential forces F_N, F_τ because of rub-impact can be expressed as follows:

$$\begin{Bmatrix} F_N \\ F_\tau \end{Bmatrix} = \begin{cases} k_c(r-\delta)^{\frac{3}{2}}\left[1+\frac{3(1-c_e^2)\dot{r}}{4\dot{r}^-}\right]\begin{bmatrix}1\\ f\end{bmatrix} & (r>\delta) \\ \mathbf{0} & (r\le\delta) \end{cases} \tag{1}$$

here, $\dot{r}$ is the velocity of disk, $\dot{r}^-$ denotes the initial impact velocity, c_e represents the restitution coefficient, and the Herz contact stiffness k_c is defined as

$$k_c = \frac{4}{3\left(\frac{1-\upsilon_1^2}{E_1}+\frac{1-\upsilon_2^2}{E_2}\right)}\left(\frac{R_1R_2}{R_1+R_2}\right)^{\frac{1}{2}} \tag{2}$$

where R_1 and R_2 are the curvature radius of disk and fixed limiter, E_1 and E_2 are the elastic modulus of disk and fixed limiter, υ_1 and υ_2 are the Poisson's ratio of disk and fixed limiter.

The rubbing force components in x-axis and y-axis of Cartesian coordinate system can be obtained as follows:

$$\begin{Bmatrix} P_x \\ P_y \end{Bmatrix} = \begin{bmatrix} -cos\varphi & sin\varphi \\ -sin\varphi & -cos\varphi \end{bmatrix}\begin{Bmatrix} F_N \\ F_\tau \end{Bmatrix} \tag{3}$$

According to formulas (1)-(3), the rubbing force can be rewritten in the following form:

$$\begin{Bmatrix} P_x \\ P_y \end{Bmatrix} = -H(r-\delta)\,\frac{4}{3\left(\frac{1-\upsilon_1^2}{E_1}+\frac{1-\upsilon_2^2}{E_2}\right)}\left(\frac{R_1R_2}{R_1+R_2}\right)^{\frac{1}{2}}\frac{(r-\delta)^{\frac{3}{2}}\left[1+\frac{3(1-c_e^2)\dot{r}}{4\dot{r}^-}\right]}{r}\begin{bmatrix}1 & -f\\ f & 1\end{bmatrix}\begin{Bmatrix} x \\ y \end{Bmatrix} \tag{4}$$

where $H(x) = \begin{cases}1, x>0\\ 0, x\le 0\end{cases}$ is called the Heaviside function.

2.3 Differential equations of motion for dual-rotor model

Based on the above analysis and mechanical model of the dual-rotor system presented in Figure.1, the system's governing equations of motion can be obtained by using Newton's law of motion:

$$\begin{cases} m_1\ddot{x}_1 + c_1\dot{x}_1 + k_1(x_1 - x_2) = F_{x1} \\ m_1\ddot{y}_1 + c_1\dot{y}_1 + k_1(y_1 - y_2) = F_{y1} - m_1 g \\ m_2\ddot{x}_2 + c_2\dot{x}_2 + k_1(x_2 - x_1) + k_2(x_2 - x_3) = m_2 e_1\omega_1\cos(\omega_1 t) \\ m_2\ddot{y}_2 + c_2\dot{y}_2 + k_1(y_2 - y_1) + k_2(y_2 - y_3) = m_2 e_1\omega_1 sin(\omega_1 t) - m_2 g \\ m_3\ddot{x}_3 + c_3\dot{x}_3 + k_2(x_3 - x_2) + k_3(x_3 - x_4) = -F_{xRI} \\ m_3\ddot{y}_3 + c_3\dot{y}_3 + k_2(y_3 - y_2) + k_3(y_3 - y_4) = -F_{yRI} \\ m_4\ddot{x}_4 + c_4\dot{x}_4 + k_3(x_4 - x_3) + k_4(x_4 - x_5) = m_4 e_2\omega_1\cos(\omega_1 t) \\ m_4\ddot{y}_4 + c_4\dot{y}_4 + k_3(y_4 - y_3) + k_4(y_4 - y_5) = m_4 e_2\omega_1 sin(\omega_1 t) - m_4 g \\ m_5\ddot{x}_5 + c_5\dot{x}_5 + k_4(x_5 - x_4) = F_{x2} \\ m_5\ddot{y}_5 + c_5\dot{y}_5 + k_4(y_5 - y_4) = F_{y2} - m_1 g \\ m_6\ddot{x}_6 + c_6\dot{x}_6 + k_5(x_6 - x_7) = -F_{xRO} \\ m_6\ddot{y}_6 + c_6\dot{y}_6 + k_5(y_6 - y_7) = -F_{yRO} - m_6 g \\ m_7\ddot{x}_7 + c_7\dot{x}_7 + k_5(x_7 - x_6) + k_6(x_7 - x_8) = m_7 e_3\omega_2\cos(\omega_2 t) + P_x \\ m_7\ddot{y}_7 + c_7\dot{y}_7 + k_5(y_7 - y_6) + k_6(y_7 - y_8) = m_7 e_3\omega_2 sin(\omega_2 t) + P_y - m_7 g \\ m_8\ddot{x}_8 + c_8\dot{x}_8 + k_6(x_8 - x_7) + k_7(x_8 - x_9) = m_8 e_4\omega_2\cos(\omega_2 t) \\ m_8\ddot{y}_8 + c_8\dot{y}_8 + k_6(y_8 - y_7) + k_7(y_8 - y_9) = m_8 e_4\omega_2 sin(\omega_2 t) - m_8 g \\ m_9\ddot{x}_9 + c_9\dot{x}_9 + k_7(x_9 - x_8) = F_{x4} \\ m_9\ddot{y}_9 + c_9\dot{y}_9 + k_7(y_9 - y_8) = F_{y4} - m_9 g \end{cases} \tag{5}$$

where e_i $(i = 1 \cdots 4)$ are defines as the mass eccentricities of different disks, respectively; $(x_i, y_i)(i = 1 \cdots 9)$ denotes the vibration displacements of different nodes, respectively; F_{x1} and F_{y1} are the force components on the rotor from ith bearing $(i = 1,2,4)$, respectively; P_x and P_y are the rubbing force components between the outer rotor and fixed limiter in the x-axis and y-axis, respectively;

It can be clearly observed from Figure 1 that (x_{Rm}, y_{Rm}) is (x_5, y_5), and (x_{Rn}, y_{Rn}) is (x_7, y_7). Hence, Equations (13) ~ (16) can be expressed in a matrix form as

$$\mathbf{M}\ddot{\boldsymbol{X}} + \mathbf{C}\dot{\boldsymbol{X}} + \boldsymbol{K}\boldsymbol{X} = \boldsymbol{F}(\boldsymbol{t}) \tag{6}$$

where $\boldsymbol{X} = \{x_1, y_1, \cdots x_9, y_9, x_w, y_w, x_b, y_b\}$ is the displacement vector. **M, C** and $\boldsymbol{K}$ denote the mass, damping and stiffness matrices, respectively. $\boldsymbol{F}(\boldsymbol{t})$ is the external force vector.

3 Numerical results and discussion

As aforementioned, ω_1 and ω_2 represent the rotational speeds of inner and outer rotors, respectively. Therefore, a parameter is defined to describe the rotational speed ratio

$$\kappa = \frac{\omega_2}{\omega_1} \tag{7}$$

where κ is greater than 0, the motion of the dual-rotor system is co-rotation; otherwise, the motion is counter-rotation. In order to verify the model with the experiments, we pay more attention to co-rotation in the paper.

The rotational speed ratio is one of the most important parameters affecting the dynamic responses of a dual-rotor system. In the case of $\omega_1 = 2000rpm$, $\omega_2 = 3160rpm$ $(\kappa = 1.58)$, the vertical vibration displacement waveform and corresponding spectrum of node 5 under unbalance-rubbing coupling faults are presented in Figure 3. For the convenience of discussion, two parameters are introduced as follows:

$$N_1 = \frac{2\pi\omega_1}{60}, N_2 = \frac{2\pi\omega_2}{60} \tag{8}$$

It can be observed from Figure 3 that when the rotational speed ratio is $\kappa = 1.58$, the spectrum are abundant, containing many frequency components, as listed in Table 1. Although the assumption that e_2 is greater than other mass eccentricities e_i $(i = 1, 2, 4)$, the amplitude of N_1 is the second larger after that of N_2 due to the higher speed and greater mass of outer rotor. Also, some combination frequency components are observed, which may demonstrate the existence of rubbing fault.

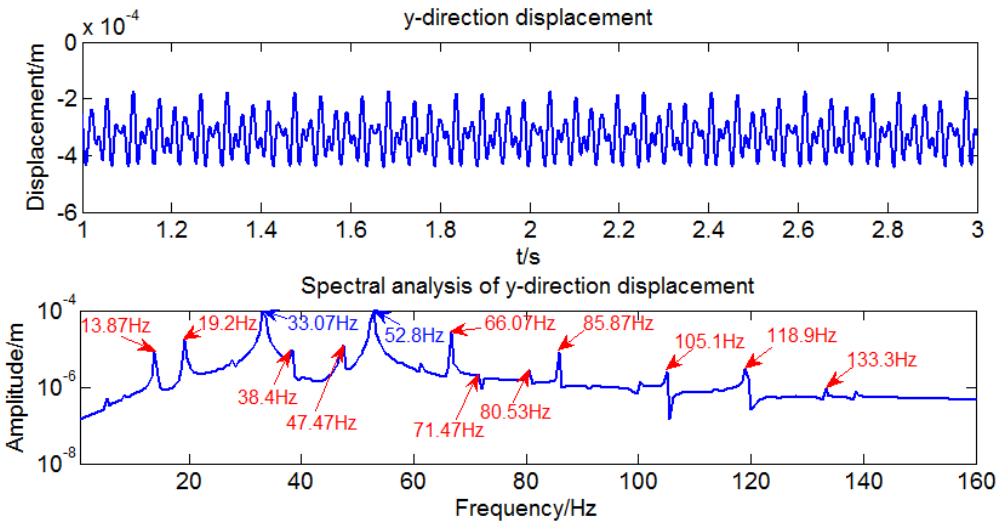

Figure 3 Vertical vibration plot and corresponding spectrum of node 5 under coupling faults (ω_1=2000rpm (33.3Hz), κ=1.58)

Table 1 Vibration frequency component analysis of node 5 (κ=1.6)

Frequency (Hz)	Component	Frequency (Hz)	Component
13.87	$2N_1 - N_2$	71.47	$2N_2 - N_1$
19.2	$N_2 - N_1$	80.53	$4N_1 - N_2$
33.07	N_1	85.87	$N_1 + N_2$
38.4	$2(N_2 - N_1)$	105.1	$2N_2$
47.47	$3N_1 - N_2$	118.9	$2N_1 + N_2$
52.8	N_2	133.3	$4N_1$
66.07	$2N_1$		

Figure 4 presents the spectrum cascade plots of the dual-rotor system utilizing the rotational speed ratio as the variable. According to the spectral depicted in Figure 4, the axis of rotational speed of inner rotor can be separated into several parts to investigate the combined frequency and others. Firstly, it can be found that with the increase of rotational speed of inner rotor, the peak values of N_1, N_2 are prominent. Secondly, the amplitudes of the combined harmonic components, such as $2N_1 - N_2$, $N_2 - N_1$, $2N_1$, always have nonzero values when rub-impact happens. Since then, the relative peaks representing the combined frequency components, such as $N_1 + 1/2\,N_2$ are obviously observed when ω_1 is greater than 272 rad/s. In particular, the frequency component, for instance $4N_1 - 2N_2$, is exhibited in the range [272, 335] rad/s.

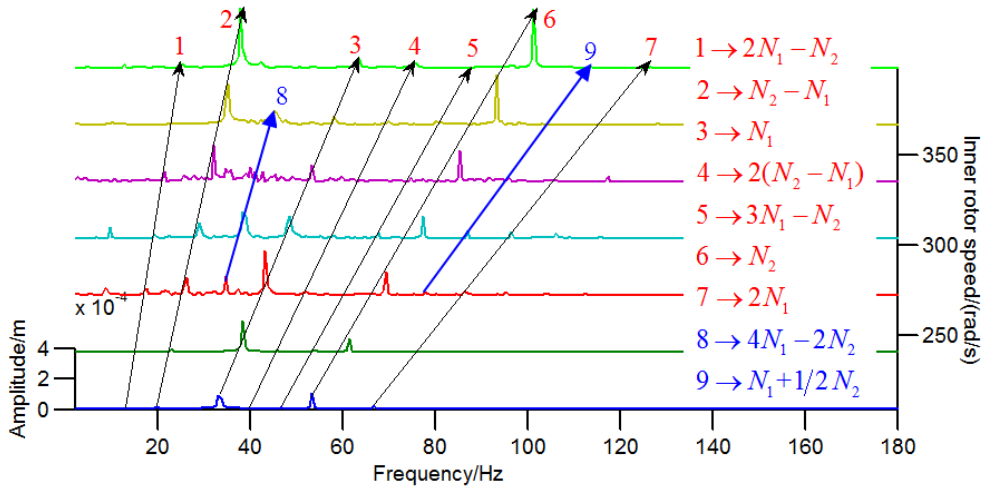

Figure 4 For κ=1.58, spectrum cascade plots of the vertical responses of node 5 under coupling faults

4 Experimental verification

4.1 Introduction to the dual-rotor experiment rig

The dual-rotor system dynamics model (see Figure 1) is set up based on the actual dual-rotor test rig. As depicted in Figure 5 (a) and (b), the dual-rotor test rig consists of key parts, such as compressor disks, turbine disks, inner and outer shafts, ball bearing and motors. According to the design of the motors, the highest rotational speed is about 18000 rpm.

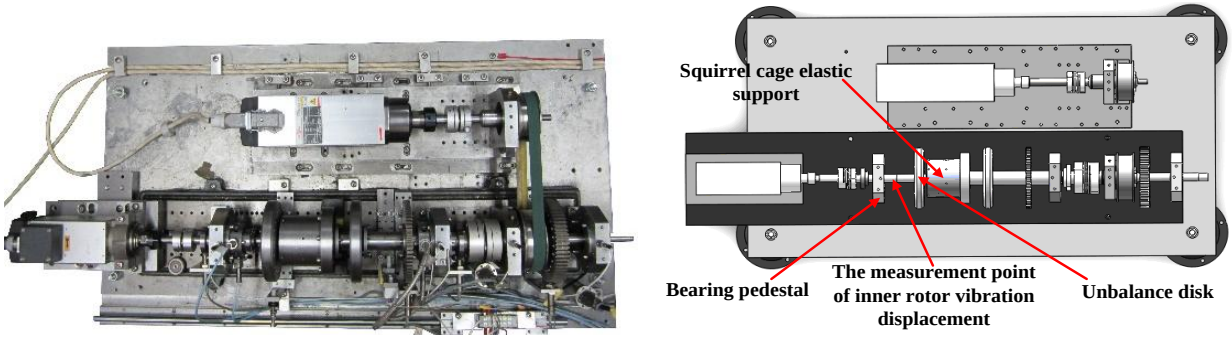

Figure 5 Structure diagram: (a) dual-rotor test rig, (b) Schematic diagram of dual-rotor system

4.2 Validity of structural model for dual-rotor system

In the condition of co-operation, the vibration responses of inner rotor under unbalance-rubbing coupling fault at different rotational speed are obtained. The sampled vibration signal and its spectrum at $\omega_1 = 2000rpm$, $\omega_2 = 3150rpm$ ($\kappa = 1.58$) is shown in Figure 6. Because of the limited influence of rubbing on the motions of rotors, the ordinate of the spectrum is expressed by using logarithmic to highlight the frequency components.

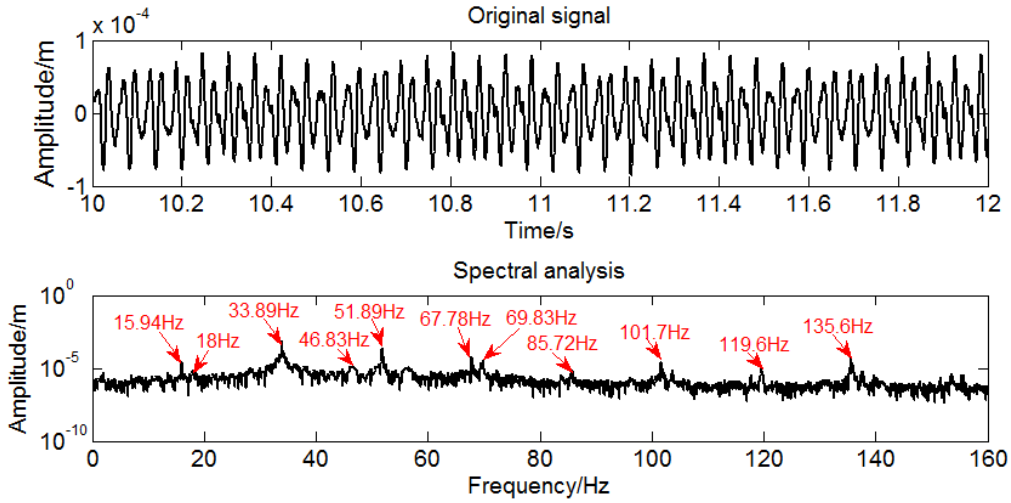

Figure 6 Vertical waveforms of inner rotor and its spectrum under unbalance-rubbing coupling faults $\omega_1 = 2000rpm\ (33.3Hz), \omega_2 = 3150rpm\ (52.5Hz)$ ($\kappa = 1.58$)

It can be observed from Figure 6 that the spectrum not only contains the fundamental frequencies of inner and outer rotor, but also contain combined frequencies of fundamental frequencies of inner and outer rotor, as shown in Table 2. Since it's difficult to adjust the dual-rotor experimental test rig to the ideal state, there are always some minor faults in the initial period, such as misalignment, pedestal looseness. Under the influence of these factors, the spectrums of inner rotor may have many frequency components with small amplitudes. By comparing Figure 3 with Figure 6, the amplitude of numerical results is approximately equal to that of experiment results.

Table 2 Vibration frequency component analysis of inner rotor

Frequency (Hz)	Component	Frequency (Hz)	Component
15.94	$2N_1 - N_2$	69.83	$2N_2 - N_1$
18	$N_2 - N_1$	85.72	$N_1 + N_2$

33.89	N_1	101.7	$3N_1$
46.83	$3N_1 - N_2$	119.6	$2N_1 + N_2$
51.89	N_2	135.6	$4N_1$
67.78	$2N_1$		

5 Conclusions

Based on dynamic model and dual-rotor experimental rig, a study on the vibration responses of a dual-rotor system with unbalance-rubbing coupling faults has been performed in the paper. In order to better describe the impact force and frictional force between the disk and the fixed limiter, the Lankarani-Nikravesh model and the Coulomb friction relationship have been utilized to perform contact analysis. According to the numerical and experimental results, some conclusions can be summarized as follow:

(1) The spectrums under unbalance-rubbing condition not only contain the rotational frequencies of inner and outer rotor, but also contain combined frequency components, namely $mN_1 + nN_2$ $(m, n = 1,2,\cdots)$, and rub-impact is the key factor resulting in the occurrence of the combined frequency components.

(2) With the increase of rotational speed ratio, the response frequencies of the dual-rotor system with unbalance-rubbing coupling faults contain much more components.

Acknowledgments

The authors would like to acknowledge the supports from the National Natural Science Foundations of China (No. 11572167). The authors are also grateful to the anonymous reviewers for their valuable comments.

References

[1]Varney P, Green I. Nonlinear phenomena, bifurcations, and routes to chaos in an asymmetrically supported rotor–stator contact system [J]. Journal of Sound & Vibration, 2015, 336(336):207-226.

[2]Muszynska A, Goldman P. Chaotic responses of unbalanced rotor/bearing/stator systems with looseness or rubs [J]. Chaos Solitons & Fractals, 1995, 5(9):1683-1704.

[3]Ahmad S. Rotor Casing Contact Phenomenon in Rotor Dynamics -- Literature Survey [J]. Journal of Vibration & Control, 2010, 16(9):1369-1377.

[4]Choi Y S. Investigation on the whirling motion of full annular rotor rub [J]. Journal of Sound & Vibration, 2002, 258(1):191-198.

[5]Beatty R F. Differentiating Rotor Response Due to Radial Rubbing [J]. Journal of Vibration & Acoustics, 1985, 107(2):151-160.

[6]Ma H, Zhao Q, Zhao X, et al. Dynamic characteristics analysis of a rotor–stator system under different rubbing forms [J]. Applied Mathematical Modelling, 2015, 39(8):2392-2408.

[7]Zhang W M, Meng G, Chen D, et al. Nonlinear dynamics of a rub-impact micro-rotor system with scale-dependent friction model [J]. Journal of Sound & Vibration, 2008, 309(3-5):756-777.

[8]O. Grāpis, V. Tamužs, N.-G. Ohlson, et al. Overcritical high-speed rotor systems, full annular rub and accident [J]. Journal of Sound & Vibration, 2006, 290(3-5):910-927.

[9]Torkhani M, May L, Voinis P. Light, medium and heavy partial rubs during speed transients of rotating ma-chines: Numerical simulation and experimental observation [J]. Mechanical Systems & Signal Processing, 2012, 29(29):45-66.

[10]Wang N, Jiang D, Yang Y, et al. Study on the diagnosis of rub-impact fault based on finite element method and envelope demodulation [J]. Journal of Vibroengineering, 2016, 18(7):4500-4512.

[11]Wang N F, Jiang D X, Han T. Dynamic characteristics of rotor system and rub-impact fault feature research based on casing acceleration [J]. Journal of Vibroengineering, 2016, 18(3):1525-1539.

[12]Patel T H, Zuo M J, Zhao X. Nonlinear lateral-torsional coupled motion of a rotor contacting a viscoelastically sus-pended stator [J]. Nonlinear Dynamics, 2011, 69(1-2):325-339.

[13]Roques S, Legrand M, Cartraud P, et al. Modeling of a rotor speed transient response with radial rubbing [J]. Journal of Sound & Vibration, 2010, 329(5):527-546.

[14]Yuan Z, Chu F, Wang S, et al. Influence of rotor's radial rub-impact on imbalance responses [J]. Mechanism & Machine Theory, 2007, 42(12):1663-1667.

[15]Popprath S, Ecker H. Nonlinear dynamics of a rotor contacting an elastically suspended stator [J]. Journal of Sound & Vibration, 2007, 308(3–5):767-784.

[16]Lu W, Chu F. Radial and torsional vibration characteristics of a rub rotor [J]. Nonlinear Dynamics, 2014, 76(1):529-549.